Meas. Sci. Technol. **19** (2008) 065204 (8pp) doi:10.1088/0957-0233/19/6/065204

Effects of inlet/outlet configurations on the electrostatic capture of airborne nanoparticles and viruses

Jaesung Jang[1], **Demir Akin**[2,3] **and Rashid Bashir**[4]

[1] Department of Mechanical Engineering, Chung-Ang University, Seoul 156-756, Korea
[2] Laboratory of Integrated Biomedical Micro/Nanotechnology and Applications, Birck Nanotechnology Center, Bindley Biosciences Center, Purdue University, West Lafayette, IN 47907, USA
[3] Weldon School of Biomedical Engineering, Purdue University, West Lafayette, IN 47907, USA
[4] Micro and Nanotechnology Laboratory, Department of Electrical and Computer Engineering and Department of Bioengineering, University of Illinois at Urbana–Champaign, Urbana, IL 61801, USA

E-mail: rbashir@uiuc.edu

Received 15 November 2007, in final form 23 April 2008
Published 19 May 2008
Online at stacks.iop.org/MST/19/065204

Abstract
Motivated by capture and detection of airborne biological agents in real time with a cantilever biosensor without introducing the agents into liquids, we present the effects of inlet/outlet configurations of a homemade particle collector on the electrostatic capture of airborne 100 nm diameter nanoparticles under swirling gas flows. This particle collector has three different inlet/outlet configurations: forward inlet/outlet (FO), backward inlet/outlet (BO) and straight inlet/outlet (SO) configurations. We also present the electrostatic capture of *Vaccinia* viruses using the same particle collector and compare these virus measurements with the nanoparticle cases. The most particles were collected in the FO configuration. The numbers of particles captured in the BO and SO configurations were close within their standard deviations. For all the three configurations tested, the number of particles captured in the center electrode C was much smaller than those captured in the other electrodes at a flow rate of 1.1 l min^{-1} and an applied potential of 2 kV. Using a commercial CFD code FLUENT, we also simulated the effects of the three inlet/outlet configurations on the particle capture in terms of particle trajectories, velocities and travel times. This simulation was in a good agreement with measurements that the FO configuration is the most favorable to particle capture among the tested configurations at a flow rate of 1.1 l min^{-1}. The effects of particle diameters on the capture will also be discussed. This collector can be used for real-time monitoring of bioaerosols along with cantilever biosensors.

Keywords: airborne nanoparticles and *Vaccinia* viruses, electrostatic capture, cantilever biosensors, swirling flows

(Some figures in this article are in colour only in the electronic version)

1. Introduction

In recent years, a large number of techniques have been developed for the collection and detection of biological aerosols such as airborne bacteria, viruses, or fungi in a wide variety of applications (Macher 1999, Yao and Mainelis 2006, Agranovski *et al* 2006, Li and Wen 2003, Horgan *et al* 2005, Fatah *et al* 2001, Hermann *et al* 2006). Typically, collected bioaerosols are examined in the gas phase or most often introduced into a liquid medium, where they can be further tested to determine the presence of specific biological targets and the concentration of the targets (Macher 1999, Fatah *et al* 2001).

Conventional detection methods of biological agents include culture and colony counting, polymerase chain reaction (PCR) or enzyme-linked immunosorbent assay (ELISA) (Macher 1999, Lazcka *et al* 2007). These tests are well established, but they require several assay steps, well-trained technical staff and a significant time to obtain reliable results (Ivnitski *et al* 1999, Dhayal *et al* 2006). Therefore, sensitive biosensors that accurately detect, in a label-free manner and in real time, are highly required (Ivnitski *et al* 1999, Lazcka *et al* 2007). Among the biosensors, cantilever-based mass sensors have been widely used in bio-medical applications due to the very high sensitivity of the cantilever structure (Lavrik and Datskos 2003, Lavrik *et al* 2004, Gupta *et al* 2004, Waggoner and Craighead 2007). They generally work better in the gas state because of higher quality factors and hence higher sensitivity than in the liquid state, which may make it unnecessary to introduce airborne microorganisms into liquids. However, the number of biological particles that can be placed on the cantilever surfaces for detection is usually very small compared to the total number of particles tested, which requires an active collection method such as electrostatic capture to increase overall sensor sensitivity.

A number of electrostatic collectors have been developed to capture bioaerosols from airstreams (Mainelis *et al* 2002, Li and Wen 2003). They usually use a corona discharger to charge incoming aerosols and then collect these charged aerosols by electrostatic forces. They have shown high collection efficiencies as high as 99% due to high electrical mobility of these multiply charged particles (Mizuno 2000). However, corona dischargers are well known to produce oxides of nitrogen and ozone, which can adversely affect viability of some airborne microorganisms (Crook 1995, Kowalski *et al* 2003, Yao and Mainelis 2006).

We presented a flow-swirling-based electrostatic particle collector without a corona discharger (Jang *et al* 2006, 2007). The advantage of this particle collector is that flow swirling makes particles stay long and slow down in the collector, which gives rise to many particles to be captured. In this paper, we will investigate the effects of the inlet/outlet configurations of the particle collector on the electrostatic capture of nanoparticles with simulation and experiments. In fact, the number of particles flowing in the collector varies spatially along the collector, depending on the inlet/outlet configurations. Therefore, it is critical to find information on where inside the collector the most particles flow because biosensors need to be exposed to as many particles as possible, especially if the biosensors involve cantilevers. We also present the capture of *Vaccinia* viruses with different flow rates in the same collector and compare these measurements with nanoparticle experiments. The highest and smallest capture positions inside the collector will be determined by these experiments. The effects of particle diameters on the electrostatic capture will also be discussed. This collector is well suited for integration with cantilever sensors for the detection of bioaerosols and can be a promising choice in terms of real-time monitoring.

2. Materials and methods

2.1. Particle generator, neutralizer and particle collector

Figure 1 shows a schematic of a particle generation system and the particle collector (Jang *et al* 2007), and its top view, which shows the three different inlet/outlet configurations, FO (i), BO (ii) and SO (iii) (Jang *et al* 2006). This collector has five metal sheets ($12 \times 12\,\text{mm}^2$) on its bottom, acting as the positive electrodes to capture negatively charged airborne nanoparticles or microorganisms, and a large grounded electrode on the top (see figure 1(*c*)).

Nanoparticles or viruses are passed through 25 or 40 μm inner diameter capillary tubes and they are aerosolized using an electrospray aerosol generator (Model 3480, TSI Inc., St Paul, MN). The generated aerosols are then neutralized by a polonium-210 source (Po-2042, NRD Inc., Grand Island, NY), resulting in the generated aerosols in charge equilibrium. According to the equilibrium charge distribution produced by the neutralizer, about 28% of the total particles 100 nm in diameter have single negative charges ($n = -1$) and 6% of the total particles have multiple negative charges. For 200 nm diameter particles, about 26% and 12% of the total particles have single negative charges and multiple negative charges, respectively (Wiedensohler 1988).

2.2. Nanoparticles and viruses

The nanoparticles and viruses we used were 100 nm diameter polystyrene fluorescent beads (R100, Duke Scientific Corp., Palo Alto, CA) and *Vaccinia* viruses, respectively. These nanoparticles and viruses were diluted with an aqueous 10 mM ammonium acetate buffer (667404, Sigma-Aldrich). The concentrations of the nanoparticle and virus solutions were 1.8×10^{11} particles ml^{-1} and 8.5×10^{10} particles ml^{-1}, respectively. *Vaccinia* viruses belong to the *Poxviridae* family and they are live viruses of smallpox vaccines. They are usually brick shaped and around $200 \times 200 \times 250\ \text{nm}^3$ (Fauquet *et al* 2005). Airborne *Vaccinia* viruses were generated with 40 μm inner diameter capillary tubes because these viruses can be generated in various sizes due to their aggregation.

2.3. Experimental procedure

A silicon chip ($10 \times 10\ \text{mm}^2$) is cleaned using a piranha solution (a mixture of H_2O_2 and H_2SO_4) and then placed on one of the bottom electrodes. After applying electric potential for a given period of time, the fluorescent nanoparticles captured on the silicon chip are imaged under an epifluorescent microscope and counted with ImageJ, free software distributed by the US National Institute of Health. As for the virus experiments, the virus suspension is first treated with ultraviolet radiation and then used for electrospray aerosol generation. The viruses captured on the silicon chip are imaged with a scanning electron microscope (SEM) and counted.

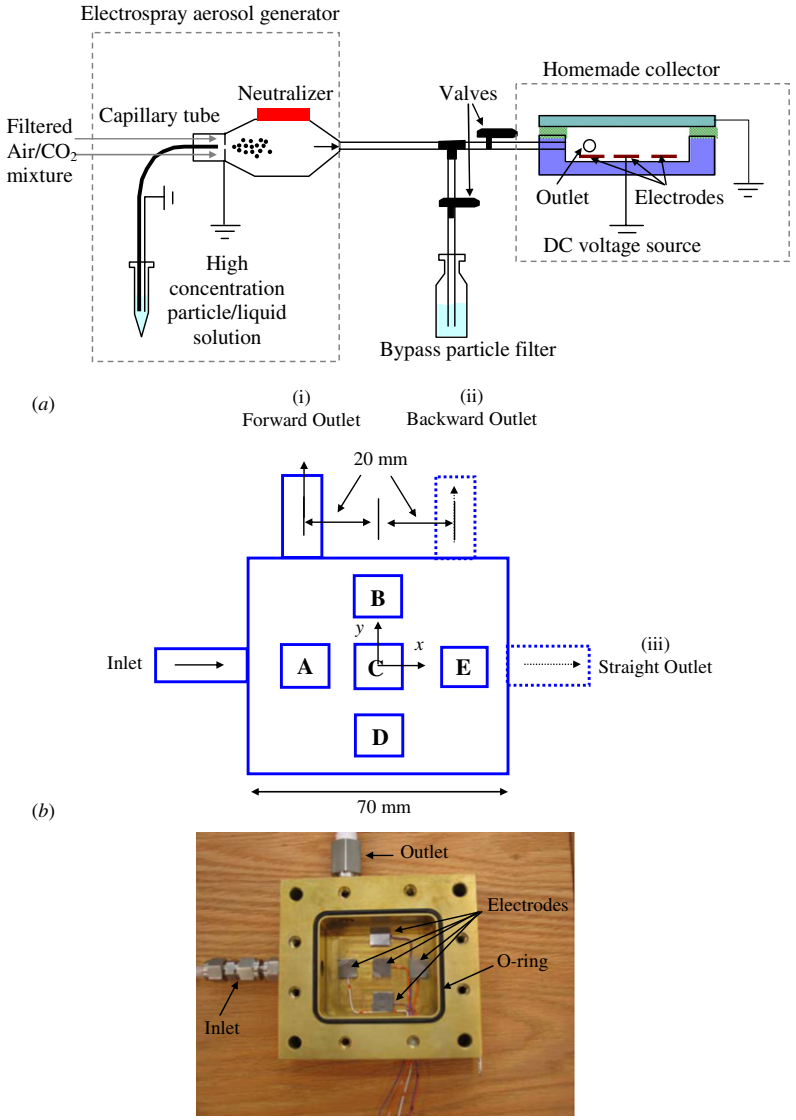

Figure 1. Schematic of a particle generation system and the particle collector (Jang *et al* 2007) (*a*), the top view of the collector, showing the three different inlet/outlet configurations (Jang *et al* 2006) (*b*) and a picture of the particle collector with the forward outlet (*c*). The capital letters in (*b*) indicate each electrode.

2.4. Computation of particle trajectories in the collector

Airborne particles flowing under non-uniform electrostatic fields will experience electrical forces, flow-induced forces, gravity, etc (Baron and Willeke 2001). In the current simulation, both flow and electric fields were obtained separately and particles were traced from flow fields without considering the effects of electric fields on the particles. These particle tracks give important information on the relationship between the particle velocities, the distance from the electrodes to the particles and the captured particle counts with the electrode position when the electrostatic forces are almost constant with the electrode positions (Jang *et al* 2007). Particle trajectories in the collector were numerically computed with the discrete phase model of a CFD code FLUENT 6.2. The flow fields were obtained based on the incompressible laminar flow model. In fact, the Reynolds numbers based on the inlet diameter are 137 and 248 at 1.1 l min^{-1} and 2.0 l min^{-1}, respectively.

3. Results and discussion

3.1. Comparison of the measured particle capture in the three inlet/outlet configurations

Figure 2 shows the number of nanoparticles captured in an area of 217.8 × 172.5 μm^2 in the three inlet/outlet configurations when the electric potential of 2 kV was applied for 20 min at 1.1 l min^{-1}. The error bars represent the standard deviations of the measurements. The flow rate of 1.1 l min^{-1} was chosen because it is recommended by TSI for the electrospray aerosol generator. Moreover, many handheld airflow devices work at a flow rate range of several liters per minute. We observed that

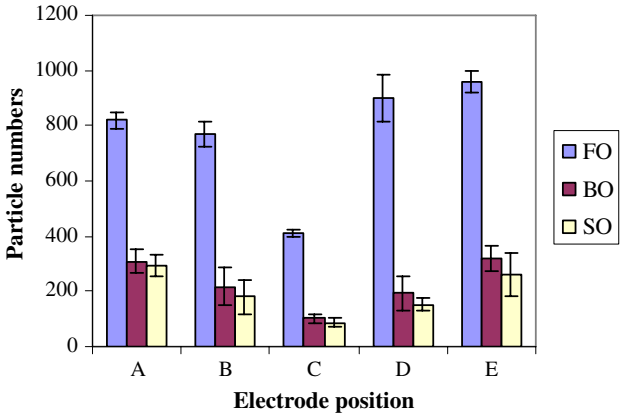

Figure 2. Total number of nanoparticles captured in an area of $217.8 \times 172.5\ \mu m^2$ on each electrode in the three inlet/outlet configurations when the electric potential of 2 kV was applied for 20 min at 1.1 l min^{-1}. The error bars represent standard deviations of the measurements.

much more particles were captured in the FO configuration than the other two configurations. In fact, the number of particles collected in the FO configuration was about 3–6 times larger than that collected in the SO configuration, depending on the electrode. We also observed that the number of particles captured in the BO configuration was slightly larger than that captured in the SO configuration although the measurements in both configurations were overlapped within their standard deviations. It is interesting that the least particles were captured in the SO configuration, which is most commonly used. For all the three configurations, the particle counts in the electrodes A, B, D and E were shown to be close within their uncertainties while the particle counts captured in the center electrode C were much less than those captured in the other surrounding electrodes. In fact, the particle counts captured on the electrode C were about 30–40% of those captured on the electrode E in the three configurations. Therefore, the center position is the last to place the biosensor for all the three configurations. We will further discuss these measurements with simulation in the next section.

3.2. Simulation on the effects of the inlet/outlet configuration

Figure 3(*a*) shows the travel times of 69 test particles (particle id: 0–68) in the particle collector at a flow rate of 1.1 l min^{-1} for the three inlet/outlet configurations. The particle id stands for particle identification number and the travel time indicates the period of time during which the test particle flows from the inlet to the outlet. These test particles were equally spaced on the inlet surface when they started flowing (Jang *et al* 2007). In the SO configuration, the travel times of all the test particles are shown to be almost the same and the median travel time is the shortest among the three configurations. In the BO configuration, about 30% of the particles have longer travel times than the other particles do, but the median travel time is not much larger than that in the SO configuration. Unlike the above two configurations, the median travel time in the FO configuration is 4–5 times longer. In fact, the median travel times of all the test particles at a flow rate of 1.1 l min^{-1} are 4.95 s, 1.40 s and 0.96 s in the FO, BO and SO configurations, respectively. That is, the particles in the FO configuration stay much longer inside the collector than those in the other configurations do, which is highly beneficial to particle capture.

It should be noticed that the smaller particle ids in figure 3(*a*) are to the right side of the inlet surface when the inlet surface is seen from the negative x side. Figures 3(*b*)–(*e*) show the trajectories of particle id of 22 in the FO (*b*) and SO (*c*) configurations and particle id of 62 in the FO (*d*) and SO (*e*) configurations. The particle ids 22 and 62 represent the smaller and larger particle ids, respectively. In the BO configuration, only the particles starting on the further right side of the inlet surface swirl in the collector before they leave the collector. In the FO configuration, many particles from the right side to the center of the inlet surface swirl in the collector (see figure 3(*b*)). On the other hand, the larger particle ids are to the left side of the inlet surface, which is closer to the outlet, and hence they move to the outlet without much swirling (see figure 3(*d*)).

We also computed the minimum horizontal velocities that each of the test particles can get when passing through the expanded volumes versus the distance of the particles from each electrode at a flow rate of 1.1 l min^{-1} in the three configurations (see figure 4). In figure 4, most of the particle collection on the electrodes happens where the particles move slowly and near the electrodes for a given electric field intensity. On the other hand, in the region where particles are flowing fast and distant from the electrodes, applied electrostatic forces may not be large enough to change the directions of the particles toward the electrodes and collect the particles (Jang *et al* 2007).

It was observed in this simulation that more particles flow slowly in the BO configuration compared to those in the SO configuration. However, particle capture measurements in both configurations were shown to be close within their standard deviations. This can be attributed to the fact that the particles in the BO configuration stay almost as long as those in the SO configuration do. In fact, if two particles flow with the same velocities at the same distance from the same electrode, the particle staying longer under the electric field will have a higher probability to be captured. Likewise, more particles in the FO configuration are shown to flow slowly than those in the BO configuration for all the electrodes. In addition, the travel times of particles in the FO configuration are much longer than those in the other configurations. This simulation shows a good agreement with the experimental data that the most particles were captured in the FO configuration. According to the experiments and simulations above, we can conclude that the FO configuration is the most advantageous to particle capture among the tested configurations.

3.3. Simulation on the effects of particle diameters

The effects of particle diameters on the electrostatic capture can be important especially for *Vaccinia* viruses because these viruses can often aggregate resulting in an increase in their

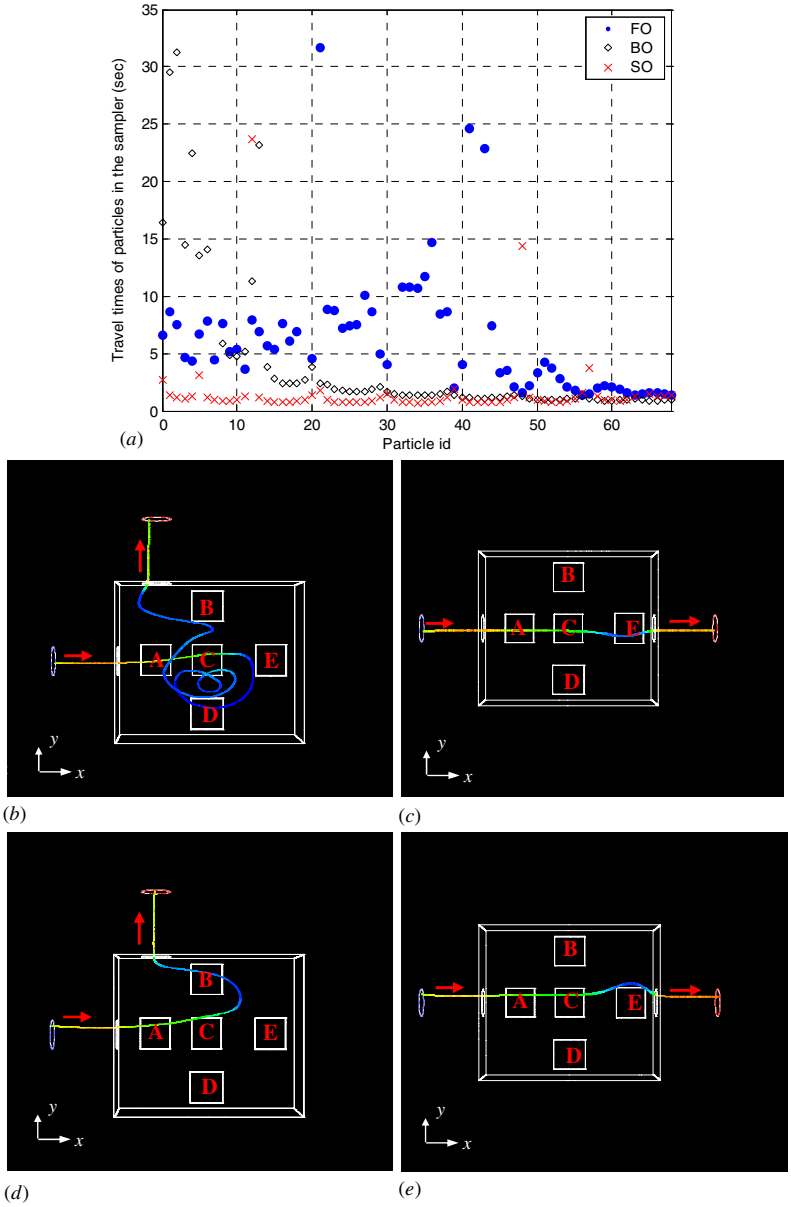

Figure 3. Travel times of 69 test particles (particle id: 0–68) in the particle collector at a flow rate of 1.1 l min^{-1} for the three inlet/outlet configurations where particle id stands for particle identification number (*a*) and trajectories of particle id of 22 in FO (*b*) and SO (*c*) configurations and particle id of 62 in FO (*d*) and SO (*e*) configurations. The medians of the travel times at a flow rate of 1.1 l min^{-1} are 4.95 s, 1.40 s and 0.96 s in the FO, BO and SO configurations, respectively.

effective particle sizes. Table 1(a) shows the number of test particles passing through volumes made up of the electrode areas and collector height for different particle sizes in the FO configuration at 1.1 l min^{-1}. The simulation shows that the number of 10 μm diameter particles flowing over the electrodes B and D decreases compared to the smaller particles, which means that the inertia of those large particles gets more important in particle transport and those particles are reluctant to swirl in the collector. The increase in inertia can also happen to the large particles flowing over the electrodes A, C and E, but these electrodes are in the straight line of the incoming flow path so the number of particles does not change as much as the electrode B and D cases. The increased inertia may cause more particle losses before the collector due to sedimentation or abrupt change in the flow path (Brockmann 2001).

3.4. Vaccinia virus capture on the electrodes

Figure 5 shows an SEM image of *Vaccinia* viruses before electrospray particle generation, which was obtained by putting a drop of virus suspension on a silicon chip and drying it, and the insets show the SEM images of two types of single *Vaccinia* virus particles captured on the electrodes C and E at 2 kV, 1.2 l min^{-1} for 30 min in the FO configuration.

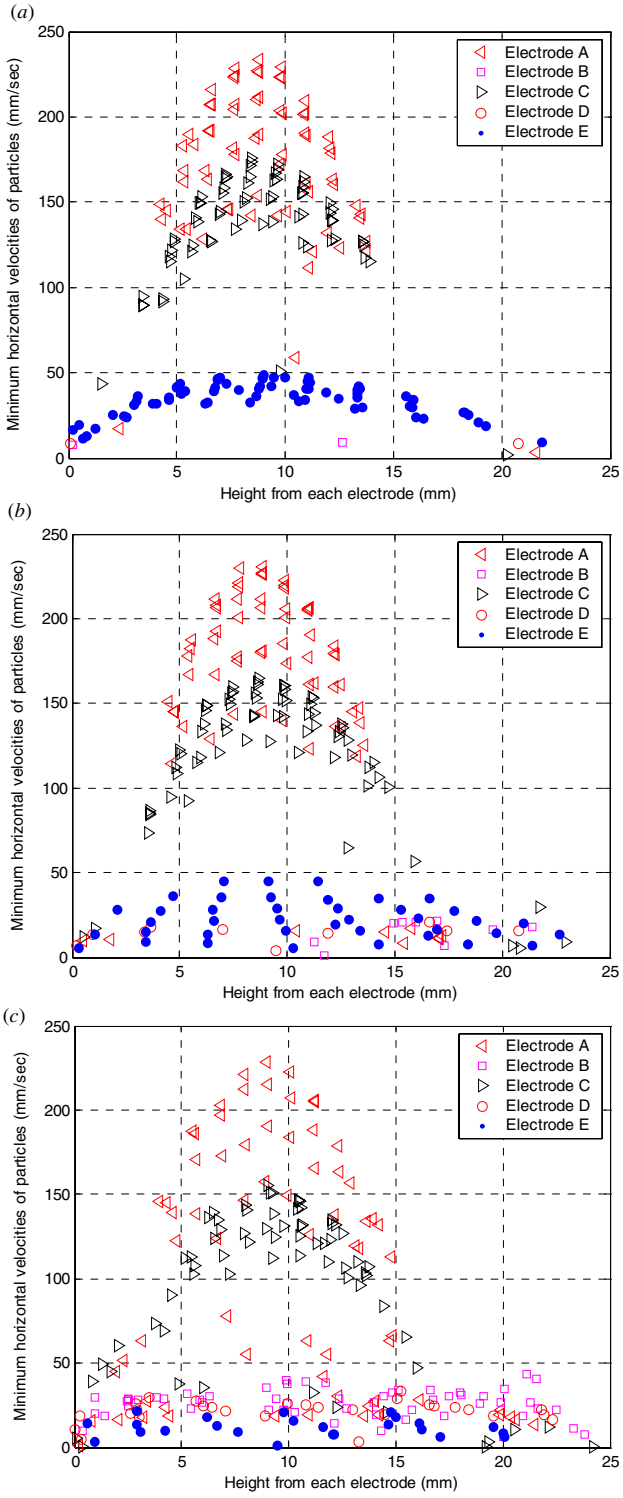

Figure 4. Minimum horizontal velocities of the particles passing through the expanded volumes versus the distance of the particles from each electrode at a flow rate of 1.1 l min^{-1} in the SO (*a*), BO (*b*) and FO (Jang *et al* 2007) (*c*) configurations.

It is observed that many of these viruses clump together as we mentioned earlier and almost all the captured viruses are shown to be intact although many of the captured viruses are

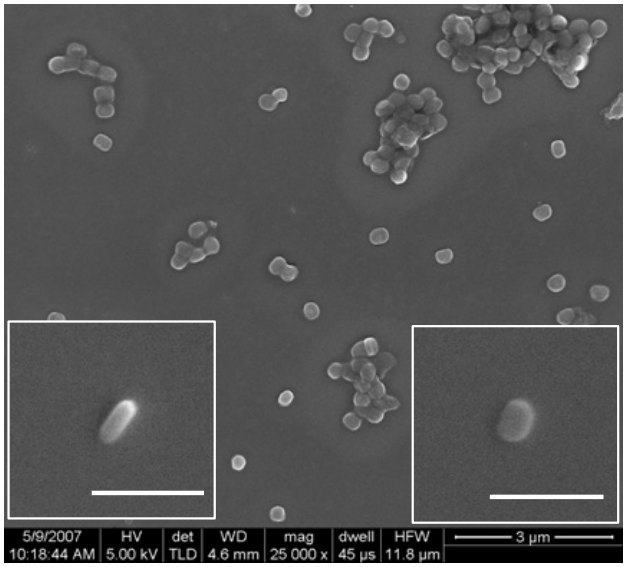

Figure 5. SEM image of *Vaccinia* viruses from virus suspension before electrospray airborne particle generation, where the insets show the SEM images of two types of single *Vaccinia* virus particles captured on the electrodes C and E at 2 kV, 1.2 l min^{-1} for 30 min in the FO configuration. The white scale bars in the insets indicate 500 nm.

Table 1. Number of test particles passing through volumes made up of the electrode areas and collector height for different particle diameters in the FO configuration at 1.1 l min^{-1} (a), and the measured number of *Vaccinia* viruses captured on the electrodes C and E at an area of 1 × 1 μm^2 at 2 kV when the total number of viruses generated at the capillary tip is 10^{12}. The numbers in the parentheses indicate the standard deviations (b).

	A	B	C	D	E
(a)					
100 nm	69 (100%)	48 (70%)	61 (88%)	27 (39%)	15 (22%)
1 μm	69 (100%)	48 (70%)	61 (88%)	26 (38%)	15 (22%)
10 μm	69 (100%)	27 (39%)	59 (86%)	17 (25%)	15 (22%)
(b)					
1.2 l min^{-1}			2.03 (0.88)		15.4 (7.42)
2.0 l min^{-1}			1.27 (0.30)		4.31 (1.06)

somewhat elongated. Figure 6 shows SEM images of *Vaccinia* viruses captured on the electrodes C (1.2 l min^{-1}) (*a*), E (1.2 l min^{-1}) (*b*), C (2.0 l min^{-1}) (*c*) and E (2.0 l min^{-1}) (*d*) at 2 kV for 30 min in the FO configuration. The electrodes C and E were chosen because these two represent the least and most particle capture electrodes, respectively, according to the aforementioned measurements and simulations. The white dots in the images indicate *Vaccinia* virus particles.

Table 1(b) shows the number of *Vaccinia* viruses captured on the electrodes C and E at an area of 1 × 1 μm^2 at 2 kV when 10^{12} *Vaccinia* virus particles are generated at the capillary tip. The numbers in the parentheses indicate the standard deviations of the measurements. Like the nanoparticle cases, the number of virus particles captured on the electrode E is larger than that captured on the electrode C and more viruses are captured at lower flow rates. The number of virus particles captured on the electrode C were about 13

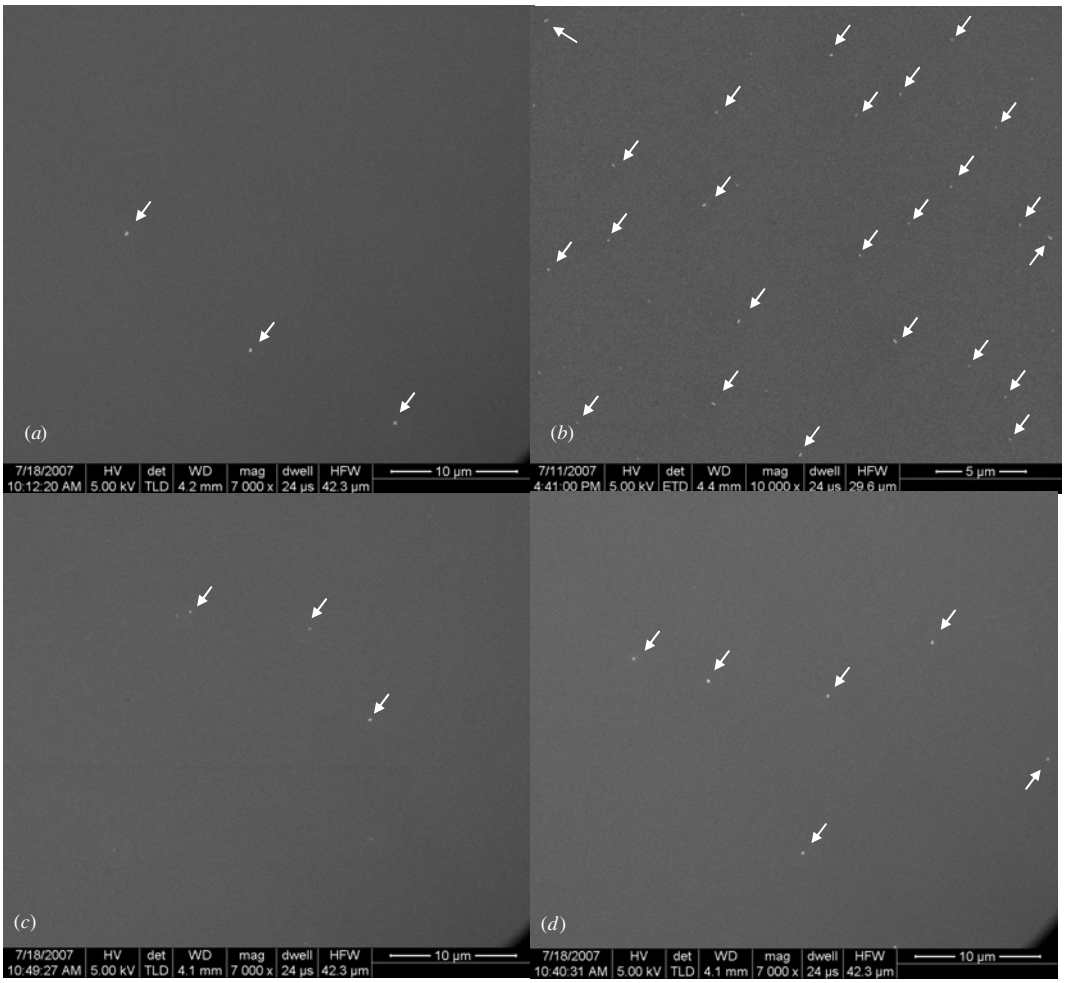

Figure 6. SEM images of *Vaccinia* viruses captured on the electrodes C (1.2 l min^{-1}) (*a*), E (1.2 l min^{-1}) (*b*), C (2.0 l min^{-1}) (*c*) and E (2.0 l min^{-1}) (*d*) at 2 kV for 30 min in the FO configuration, where the arrows point to *Vaccinia* virus particles.

and 29% of those captured on the electrode E at 1.2 and 2.0 l min^{-1}, respectively. It is interesting that less *Vaccinia* viruses are captured compared to the nanoparticles. In fact, the viruses are captured 3–11 times less than the nanoparticles are, depending on the electrode and flow rates. One of the possible reasons is that these viruses may be polydisperse rather than monodisperse when they become airborne from the suspension. Consequently, larger particles may drop before they reach the particle collector or they may be less attracted to the electrodes in the collector because of their larger inertia.

4. Conclusions

We presented the effects of the inlet/outlet configurations on the electrostatic capture of airborne 100 nm diameter nanoparticles using a homemade particle collector toward our goal of capturing and detecting airborne biological entities using a cantilever biosensor. The measurements showed that the most particles were captured in the FO configuration and the number of particles captured in the BO and SO configurations was close within their standard deviations. For all the three configurations, the number of particles captured in the center electrode C was much smaller than those captured in the other electrodes at a flow rate of 1.1 l min^{-1}. We also simulated the effects of the three inlet/outlet configurations on the particle capture in terms of particle trajectories, velocities and travel times in the collector. These simulations were consistent with measurements. That is, the FO configuration is the most favorable to particle capture among the tested configurations at a flow rate of 1.1 l min^{-1}. The effects of particle diameters on the capture were also discussed. The larger particles got more reluctant to swirl in the collector due to their increased inertia.

We also presented the capture of airborne *Vaccinia* viruses using the same particle collector in the FO configuration. In the measurements, the number of viral particles captured on the electrode E was larger than that captured on the electrode C, which is in agreement with the nanoparticle cases. On the other hand, less virus particles were captured than the nanoparticles. Work is continuing to integrate a microscale sensor for the detection of the airborne viral particles along with real-time capture.

Acknowledgments

The authors would like to thank Prof. Michael R. Ladisch for fluorescence measurements and Dr Stanley Kaufman at TSI for his valuable advices on the electrospray aerosol generator. The authors would also like to thank Dr Debby Sherman for assistance with SEM imaging. The authors are also thankful for the financial support of the US National Institute of Health (NIBIB grant number R21/R33 EB00778-01) for funding Dr Demir Akin and Dr Jaesung Jang.

References

Agranovski I E, Safatov A S, Sergeev A A, Pyankov O V, Petrishchenko V A, Mikheev M V and Sergeev A N 2006 Rapid detection of airborne viruses by personal bioaerosol sampler combined with the PCR device *Atmos. Environ.* **40** 3924–9

Baron P A and Willeke K 2001 Gas and particle motion *Aerosol Measurement: Principles, Techniques, and Applications* 2nd edn ed P A Baron and K Willeke (New York: Wiley)

Brockmann J E 2001 Sampling and transport of aerosols *Aerosol Measurement: Principles, Techniques, and Applications* 2nd edn ed P A Baron and K Willeke (New York: Wiley)

Crook B 1995 Non-inertial samplers: biological perspectives *Bioaerosols Handbook* ed C S Cox and C M Wathes (Boca Raton, FL: Lewis)

Dhayal B, Henne W A, Doorneweerd D D, Reifenberger R G and Low P S 2006 Detection of *Bacillus subtilis* spores using peptide-functionalized cantilever arrays *J. Am. Chem. Soc.* **128** 3716–21

Fatah A A, Barrett J A, Arcilesi R D Jr, Ewing K J, Lattin C H and Moshier T F 2001 *An Introduction to Biological Agent Detection Equipment for Emergency First Responders: NIJ Guide 101-00* (Washington, DC: National Institute of Justice)

Fauquet C M, Mayo M A, Maniloff J, Desselberger U and Ball L A 2005 *Virus Taxonomy: Classification and Nomenclature of Viruses* (Amsterdam/New York: Elsevier/Academic)

Gupta A, Akin D and Bashir R 2004 Single virus particle mass detection using microresonators with nanoscale thickness *Appl. Phys. Lett.* **84** 1976–8

Hermann J R, Hoff S J, Yoon K J, Burkhardt A C, Evans R B and Zimmerman J J 2006 Optimization of a sampling system for recovery and detection of airborne porcine reproductive and respiratory syndrome virus and swine influenza virus *Appl. Environ. Microbiol.* **72** 4811–8

Hogan C J Jr, Kettleson E M, Lee M-H, Ramaswami B, Angenent L T and Biswas P 2005 Sampling methodologies and dosage assessment techniques for submicrometre and ultrafine virus aerosol particles *J. Appl. Microbiol.* **99** 1422–34

Ivnitski D, Abdel-Hamid I, Atanasov P and Wilkins E 1999 Biosensors for detection of pathogenic bacteria *Biosens. Bioelectron.* **14** 599–624

Jang J, Akin D, Lim K S, Broyles S, Ladisch M R and Bashir R 2007 Capture of airborne nanoparticles in swirling flows using non-uniform electrostatic fields for bio-sensor applications *Sensors Actuators* B **121** 560–6

Jang J, Akin D, Lim K S, Ladisch M R and Bashir R 2006 Electrostatic capture of airborne nanoparticles in swirling flows for bio-MEMS applications *Proc. IMECE 2006 Paper No. IMECE2006-15411*

Kowalski W J, Bahnfleth W P, Striebig B A and Whittam T S 2003 Demonstration of a hermetic airborne ozone disinfection system: studies on *E. coli Am. Ind. Hyg. Assoc. J.* **64** 222–7

Lavrik N V and Datskos P G 2003 Femtogram mass detection using photothermally actuated nanomechanical resonators *Appl. Phys. Lett.* **82** 2697–9

Lavrik N V, Sepaniak M J and Datskos P G 2004 Cantilever transducers as a platform for chemical and biological sensors *Rev. Sci. Instrum.* **75** 2229–53

Lazcka O, Del Campo F J and Munoz F X 2007 Pathogen detection: a perspective of traditional methods and biosensors *Biosens. Bioelectron.* **22** 1205–17

Li C-S and Wen Y-M 2003 Control effectiveness of electrostatic precipitation on airborne microorganisms *Aerosol Sci. Technol.* **37** 933–8

Macher J 1999 *Bioaerosols: Assessment and Control* (Cincinnati, OH: ACGIH)

Mainelis G, Willeke K, Adhikari A, Reponen T and Grinshpun S A 2002 Design and collection efficiency of a new electrostatic precipitator for bioaerosol collection *Aerosol Sci. Technol.* **36** 1073–85

Mizuno A 2000 Electrostatic precipitation *IEEE Trans. Dielectr. Electr. Insul.* **7** 615–24

Waggoner P S and Craighead H G 2007 Micro- and nanomechanical sensors for environmental, chemical, and biological detection *Lab Chip* **7** 1238–55

Wiedensohler A 1988 Technical note: an approximation of the bipolar charge distribution for particles in the submicron size range *J. Aerosol Sci.* **19** 387–9

Yao M and Mainelis G 2006 Utilization of natural electrical charges on airborne microorganisms for their collection by electrostatic means *J. Aerosol Sci.* **37** 513–27